18

Iterative Noise Reduction in Digital Holographic Microscopy

Victor Arrizón[1], Ulises Ruiz[1] and Maria Luisa Cruz[2]
[1]*Instituto Nacional de Astrofísica, Optica y Electronica,*
[2]*Universidad del Istmo, Oaxaca,*
México

1. Introduction

Digital holographic microscopy (DHM) is an optical technique useful to retrieve quantitative information of microscopic objects with subwavelength axial accuracy (Haddad et al., 1992; Zhang-Yamaguchi, 1998; Pedrini et al., 1999; Ferraro et al., 2005). An important feature of DHM is its non-invasive character that allows the appropriate study of microorganisms in vivo (Car et al., 2004; Marquet et al., 2005; Rappaz et al., 2005, Colomb et al., 2006; Javidi et al., 2006; Charrière et al., 2006). Some DHM setups employ microscope objectives to form the image of the object (Ferraro et al., 2003; Mann et al., 2005; Colomb et al., 2006). However, it is also possible to implement DHM in a lensless setup, where the light field scattered from the object is used instead of its projected image (Wagner et al., 1999; Schnars-Juptner, 2002; Repetto et al., 2004; Cruz et al., 2008; Oh et al., 2010). A conventional setup in DHM is based on the use of an external reference wave (RW), which interferes with the field generated by the object, forming an intensity pattern which is known as hologram of the field (Takeda et al., 1982; Kreis, 1986; Yamaguchi-Zhang, 1997; Yamaguchi et al., 2001; Arrizón-Sanchez, 2004; Liebling, 2004; Quian, 2006; Meneses-Fabian, 2006; Guo, 2007; Cruz et al., 2009). Alternately, it is possible to omit the external RW, with a consequent simplification of the optical setup (Pedrini, 1998; Xu, 2002; Javidi, 2005; Morlens, 2006; Garcia-Sucerquia, 2006; Hwang-Han, 2007; Singh-Asundi, 2009). In any case, either the object hologram or the intensity of the field scattered by object are recorded with an electronic intensity meter, such as a charge-coupled device (CCD). As a final step of DHM, the recorded object hologram (and other intensity patterns) are digitized and processed in a computer, with the aim of reconstructing the microscopic features of the object.

In this chapter we first discuss the lensless setup that employs an off-axis RW, which is known as "lensless off axis digital holography" (LOADH) setup. We also consider a more simplified optical setup, which omits both the lens and the external RW. We refer to this system using the expression "referenceless on axis digital holography" (RLOADH) setup. In RLOADH it is still possible and convenient to split the field propagated from the object into a non scattered field and a scattered field. Even when the non scattered field is not added externally, it is often identified as a RW.

The LOADH and RLOADH approaches employ fewer optical components, and tend to be cheaper and more robust, than other DHM setups. In consequence, the necessity of special

considerations to compensate the influence of imperfections of multiple optical components is reduced in LOADH and RLOADH. In both simplified approaches the presence of the RW (external and internal respectively), generates a hologram which is formed by three terms, namely: the object term, its complex conjugate, and the zero order term. The goal of the digital reconstruction process is to obtain the complex object field from the hologram intensity pattern. This process is usually facilitated by using additional information, e. g. a constraint in the object plane. In the case of the LOADH it is also possible to measure, in addition to the hologram, the intensity patterns generated by the RW and by the object field. These two intensity patterns allow the elimination of the zero order in the hologram modulation.

If the spatial frequency bandwidth (BW) of the object under study is small enough, the isolation of the object field term can be performed (at least in the LOADH procedure) by employing the Fourier domain spatial filtering (FDSF) (Takeda, 1982). However, if DHM is used to study microscopic samples of large BW, the isolation of the object field component, in the hologram, cannot be realized by this simple spatial filtering procedure. In this case, one of the useful procedures is to perform the elimination of non desired hologram components by iterative procedures (Fienup, 1987; Cederquist et al., 1989; Wu, 2004; Denis et al., 2005; Hwang-Han, 2007; Nakamura, 2007).

In this chapter we describe an iterative method that effectively recovers the object field component from the recorded hologram, in both the LOADH and RLOADH setups. In both cases, it is required to implement multiple field propagations from the hologram plane to the object plane, and vice verse. In each one of these planes, specific amplitude constraints are applied. The constraint in the hologram plane is the recorded hologram amplitude itself. On the other hand, we assume that in the object plane the field is different to zero only within the area of a binary transmittance pupil.

In order to avoid stagnation during iterations, and to ensure that convergence provides the information of the true object, with low error, we generate an initial good approximation to the object field. To obtain an appropriate initial reconstruction in the LOADH setup, applied to the reconstruction of high BW objects, we measure the intensities of the fields generated by the RW and the object field, in addition to the hologram intensity. With this information we eliminate the zero order term in the hologram modulation. As a second step we generate the initial object field reconstruction using a modified FDSF procedure. In the case of the RLOADH approach we assume that the pupil (or support) at the object plane is known. Thus we can compute digitally the field that propagate to the CCD plane from the pupil alone. We combine this information with the intensity of the field propagated from the test object, to obtain digitally a modified hologram which essentially contains the object field and a noise field. When we back-propagate this modified hologram to the object plane, the object field appears well defined (focused) at this plane, while the noise term appears defocused. Thus we obtain, within the pupil area, the object field distorted with certain amount of noise.

The approximate object field reconstruction, obtained with the described procedures, is used as the input of an iterative error reduction algorithm, which is successful in reducing the reconstruction error. A key aspect of this algorithm is a gradual application of the amplitude constraints, at the object and CCD planes. We illustrate the proposed methods by means of numerical simulations. In particular we evaluate the convergence of the iterative procedure and the fidelity of the reconstructed object field.

2. Lensless off-axis digital holography with external reference wave

The LOADH optical setup, schematically depicted in Fig. 1, is a Mach-Zender type interferometer, which is convenient for the study of transparent objects. Lenses L1 and L2 are employed only to expand and collimate the laser beam. The interferometer itself is a lensless module. It is assumed that the object to be studied is limited by a small circular pupil whose transmittance is denoted p(x,y). The object, which appears at the lower branch of the interferometer, is illuminated by an expanded and collimated laser gaussian beam, of wavelength λ. If the width of this beam is large in comparison to the pupil size, it is considered as a plane wave inside this pupil.

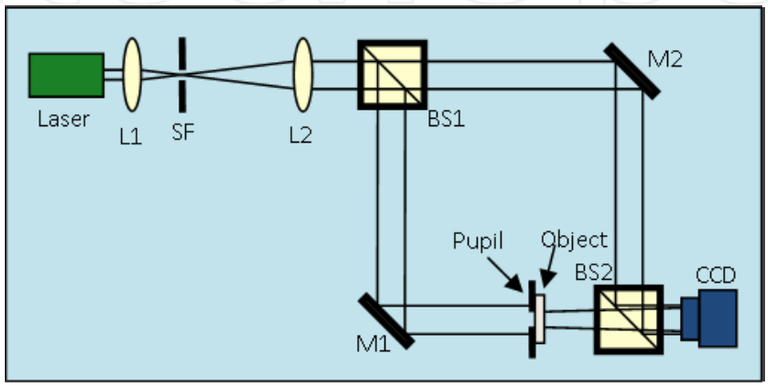

Fig. 1. LOADH optical setup. The components are: Laser, Lenses (L_1,L_2), spatial filter (SF), beam splitters (BS_1, BS_2), mirrors (M_1, M_2) and CCD.

For simplicity we assume that the object only modulates the phase of the illuminating beam. Thus, considering that the beam amplitude is normalized, the field transmitted at the object plane is

$$f(x,y) = p(x,y)\exp[i\phi(x,y)]. \tag{1}$$

This object field, freely propagated to the CCD plane, or hologram plane, is expressed as

$$g(x,y) = |g(x,y)|\exp[i\psi(x,y)]. \tag{2}$$

This field, obtained with the exact angular spectrum (AS) approach (Goodman, 1996), is mathematically represented as

$$g(x,y) = \Im^{-1}[F(u,v)H(u,v)]. \tag{3}$$

In Eq. (3), F(u,v) is the Fourier transform of f(x,y), $\Im^{-1}$ denotes the inverse Fourier transformation, and H(u,v) is the propagation factor

$$H(u,v) = \exp\left[ikz\sqrt{1-\lambda^2(u^2+v^2)}\right], \tag{4}$$

where z is the propagation distance, $k=2\pi/\lambda$, and $i=\sqrt{-1}$.
The propagated field computed with the AS approach is exact in the context of the scalar wave equation. Another advantage of the AS method is that when the operations of Eq. (3)

are performed with a fast Fourier transform (FFT) algorithm, the sampling resolution of functions f(x,y) and g(x,y) are identical. It must be noted that the propagation factor H(u,v) can be appropriately sampled more easily if the propagation distance z tends to be small. Thus, the AS approach is convenient to study high bandwidth objects (i. e. microscopic objects), for which the required distance from the CCD to the object plane is relatively short.
The reference beam, which propagates in the upper branch of the setup, is redirected to the CCD by the beam splitter BS_2. We assume that this beam is a plane wave that arrives with a slight tilt to the CCD. This RW is given by

$$r(x,y)=|r(x,y)|\exp[i2\pi(u_0x+v_0y)], \tag{5}$$

where the tilt is determined by the spatial frequencies (u_0,v_0). In this representation of the RW, the amplitude $|r(x,y)|$ can be spatially variable in the CCD area.
The superposition of the object field f(x,y) with the RW r(x,y) at the CCD plane, generates an intensity pattern, or hologram, which is given by

$$h(x,y)=|r(x,y)|^2+|g(x,y)|^2+g^*(x,y)\,r(x,y)+g(x,y)\,r^*(x,y), \tag{6}$$

where the asterisk denotes complex conjugation. The fourth term in h(x,y) contains the information of the object field, modulated by the plane wave r*(x,y). The task of DHM is to obtain the information of the object field, g(x,y), from the measured intensity h(x,y). To facilitate this purpose it is convenient to measure the intensities $I_r=|r(x,y)|^2$ and $I_g=|g(x,y)|^2$. Each one of these intensities is measured by blocking one of the branches of the interferometer. Considering these intensities together with h(x,y) we can compute the modified hologram

$$h_m(x,y)=\frac{h(x,y)-I_r-I_g}{I_r^{1/2}}. \tag{7}$$

The division by $(I_r)^{1/2}$ in Eq. (7) can be performed for the intensities measured by the CCD, making the reasonable assumption that $I_r\neq 0$ in the CCD area. Performing the operations in Eq. (7), the modulation of the modified hologram can be expressed as

$$h_m(x,y)=g(x,y)\exp[-i2\pi(u_0x+v_0y)]+g^*(x,y)\exp[i2\pi(u_0x+v_0y)]. \tag{8}$$

As noted in Eq. (8), the modulation of the modified hologram, $h_m(x,y)$, which is computed only from intensity measurements in the CCD, is formed by the object field g(x,y) and its conjugate pair, which are modulated by linear phase factors. The Fourier transform of this modified hologram, given by

$$H_m(u,v)=G(u-u_0,v-u_0)+G^*(-u-u_0,-v-u_0), \tag{9}$$

presents the function G, which is the Fourier spectrum of the object field, and its conjugated G*, placed at different positions in the Fourier domain of the hologram. It is remarkable that if these functions G and G* are not overlapped, it is possible to apply a spatial filtering that eliminates the conjugate term leaving alone the term $G(u-u_0, v-v_0)$. By centering this function it is obtained G(u,v), from which it is possible to recover the field, at the object plane, performing the inversion of Eq. (3), by means of the operation

$$f(x,y)= \Im^{-1}\left[G(u,v)H^{-1}(u,v)\right]. \tag{10}$$

The object field reconstruction, with the FDSF method described above, generates an accurate reconstructed field, only if the object bandwidth BW_{OB} is smaller than $2(u_0^2+v_0^2)^{1/2}$, otherwise the spectra bands of G and G* may appear overlapped. On the other hand, the frequency bandwidth of the CCD, given by $BW_{CCD}=p^{-1}$, being p the pixel pitch of the CCD, also restricts the object BW. For simplicity we assume that the pixel pitch is the same in the horizontal and the vertical axes of the CCD. The Fourier transform of the sampled version of the hologram $h_m(x,y)$, recorded by the CCD, is formed by multiple shifted replicas of the Fourier spectrum $H_m(u,v)$ that are repeated with periodicity BW_{CCD}. Considering the structure of $H_m(u,v)$ in Eq. (9), a convenient distribution of the multiple spectra terms G and G* in the Fourier domain of the sampled hologram is obtained adopting the carrier spatial frequencies $u_0=v_0=BW_{CCD}/4$. In this case the multiple spectra terms G and G* appear uniformly distributed in the hologram Fourier domain (Fig. 2), propitiating a reduced noise in the main object field spectrum term G, which is centered at frequency coordinates (u_0,v_0).

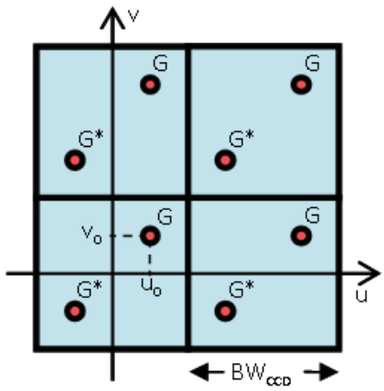

Fig. 2. Distribution of multiple spectra terms G and G* in the Fourier transform of the sampled version of the hologram $h_m(x,y)$, recorded by the CCD. This spatial distribution is uniform by using a RW with spatial frequencies $u_0=v_0=BW_{CCD}/4$.

Considering the spatial frequencies $u_0=v_0=BW_{CCD}/4$, the restriction previously established for the object BW, takes the form

$$BW_{OB}<BW_{CCD}/\sqrt{2}\,. \tag{11}$$

On the other hand, the spatial frequency bandwidth of the field must be limited so that the propagated field is captured by the CCD. This condition can be expressed as

$$BW_{OB} < 2\,\lambda^{-1}\,\sin(\theta_{max})\,, \tag{12}$$

where θ_{max} (shown in Fig. 3) is the angle subtended from the border of the CCD to the center of the object pupil.

The object reconstruction using the FDSF method will show small error if BW_{OB} is much smaller than the limits established in Eqs. (11) and (12). It is expected that the reconstruction error increases significantly when BW_{OB} is equal or greater than these limits. In the next subsections we perform numerical simulations corresponding to both cases.

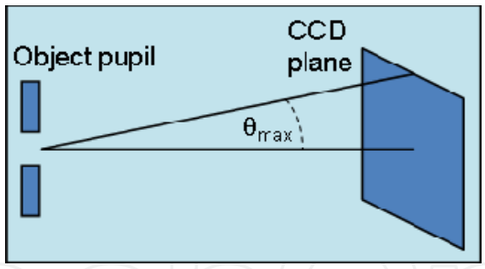

Fig. 3. The maximum angle θ_{max}, subtended from the border of the CCD to the center of the object pupil, also restricts the object bandwidth.

2.1 Reconstruction of a low bandwidth object

For the numerical simulations on DHM employing the LOADH setup we assume that the CCD has 1024x1024 pixels and pixel pitch p=5μm, which corresponds to a CCD band width BW_{CCD}=0.2 μm^{-1}. In addition, it is assumed that the distance from the CCD to the object plane is z=45 mm and that the wavelength is λ=500 nm.

We will consider first the computational reconstruction of an object with low frequency BW. The test object is an array of micro lenses, limited by a circular pupil of radius R=1mm. Each micro lens has a focal length f=30 mm and is contained in a square of width w_L=155 μm. The estimated BW of the array of lenses is obtained by the relation $BW_{OBJ}=(2)^{1/2}\ w_L\ (\lambda f)^{-1}$ (Arrizón et al., 2000). Considering the above specified parameters, one obtains $BW_{OBJ}\cong 0.015\mu m^{-1}$. On the other hand, for the determination of the RW defined in Eq. (5), we assume that the modulus is $|r(x,y)|=1$, and that the spatial frequencies are $u_0=v_0=BW_{CCD}/4$. For these parameters the object BW is much smaller than the limits given by the inequalities in Eqs. (11) and (12). For computational purposes, the object is sampled with a resolution of 5μm, which is equal to the CCD pixel pitch. In addition, the object matrix is centered in an extended (zero-padded) matrix of 1024x1024 pixels. The phase modulation within the object pupil is shown in Fig. 4 (a), and the amplitude (modulus) of the object field g(x,y), propagated to the CCD plane, is displayed in Fig. 4 (b). The amplitude values in the gray-levels bar of Fig. 4 (b) are normalized to the unitary amplitude of the beam that illuminates the test object. This type of normalization is also employed in subsequent sections.

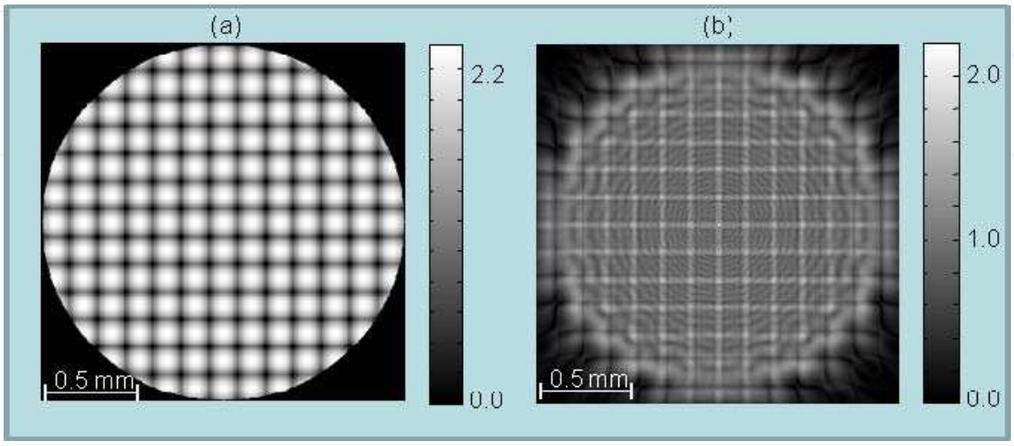

Fig. 4. (a) Phase modulation (radians) of the test object, formed by an array of micro-lenses, and (b) amplitude of the field propagated to the CCD plane.

Considering the RW, computed with Eq. (5), and the object field we obtain the hologram intensity h(x,y) and the modified hologram $h_m(x,y)$ [Eq. (8)]. In Fig. 5 we display the real valued modulation of $h_m(x,y)$ and the modulus of its Fourier spectrum $H_m(u,v)$. The object field term and its conjugate appear clearly separated in Fig. 5 (b). The object field spectrum $G(u-u_0,v-v_0)$ is placed at the left-top corner in Fig. 5 (b).

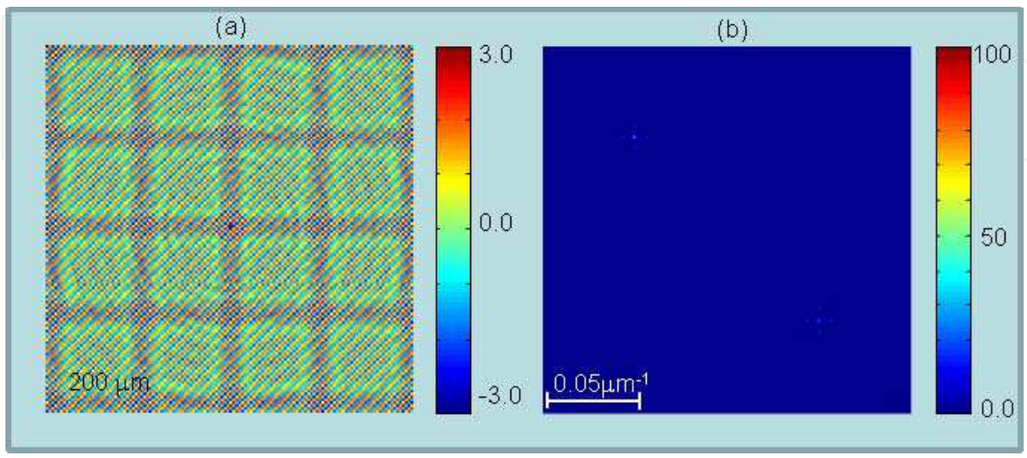

Fig. 5. (a) Close view of the real valued modulation of modified hologram $h_m(x,y)$, and (b) modulus of its Fourier spectrum $H_m(u,v)$.

The next steps are the digital elimination of the conjugate term $G^*(-u-u_0,-v-v_0)$, the centering of the field spectrum $G(u-u_0,v-v_0)$, and the inverse Fourier transformation of the centered spectrum. The result is the reconstructed object field, at the hologram plane, which we denote as $g_R(x,y)$. The reconstructed field at the object plane, denoted $f_R(x,y)$, is computed by the operations in Eq. (10), replacing $g_R(x,y)$ instead of g(x,y). The unwrapped phase of the recovered field $f_R(x,y)$ is displayed in Fig. 6(a). The reduced phase error $\arg\{f_R(x,y)\}-\arg\{f(x,y)\}$, shown in Fig 6(b), is an indicator of the high reconstruction fidelity. The discussed reconstruction process, based on the use of the FDSF technique, was presented to put in context the reconstruction of high BW objects that will be discussed in following sections.

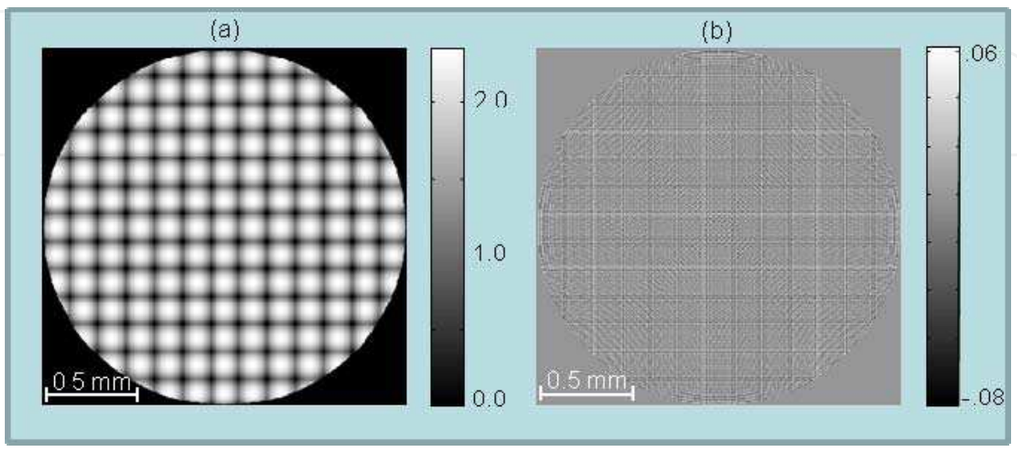

Fig. 6. (a) Unwrapped phase modulation (radians) of the reconstructed object $f_R(x,y)$, and (b) phase error $\arg\{f_R(x,y)\}-\arg\{f(x,y)\}$.

2.2 Reconstruction of high bandwidth objects

In the example of section 2.1 the FDSF is employed successfully to reconstruct a low BW object field using the LOADH setup. The use of an iterative error reduction for the reconstruction of a high BW object in the LOADH setup, is next studied. Let us consider a second test object formed by an array of micro-lenses, whose only difference with the array considered in subsection 2.1, is a new focal length f=3mm. In the LOADH setup we assume the CCD distance z=40 mm. The new estimated object BW is 0.15μm^{-1} which is 25% smaller than the CCD BW. The wrapped phase modulation of the array of lenses is shown in Fig. 7.

For the considered object, the modified hologram $h_m(x,y)$ has a wider Fourier spectrum $H_m(u,v)$, in comparison to the case discussed in section 2.1. The modulus of $H_m(u,v)$, displayed in Fig. 8 (a), shows the object field contribution (top-left corner) partially overlapped with the conjugate term (bottom-right corner). In addition, the object Fourier spectrum term overflows the limits of the spectrum window obtained with the FFT algorithm, making difficult the implementation of the spatial filtering. A solution to this problem is obtained by introducing an additional modification into the hologram $h_m(x,y)$. This change, obtained by multiplying the original modified hologram with the phase modulation of the RW, leads to the new modified hologram

$$h_m(x,y) = g(x,y) + g^*(x,y)\exp[i4\pi(u_0x + v_0y)]\,. \tag{13}$$

To obtain this new hologram modulation it is only required the knowledge of the reference wave. The spatial frequencies (u_0,v_0) of the RW can be determined, for example, by measuring the center of the object field spectrum term in the hologram Fourier domain (Cruz et al., 2009). The function $|H_m(u,v)|$, corresponding to the new hologram $h_m(x,y)$, is displayed in Fig. 8 (b), where the object spectrum term appears centred at the spectrum window. Of course, the overlapping with the conjugate term is still present. This conjugate term now has been splitted, and appears at the corners of the spectrum window. The diameter of the circle in Fig. 8 (b) is equal to the nominal object BW. For the implementation of the FDSF the Fourier spectrum field outside this circle is eliminated. This spatial filtering is a little deficient since the spectrum domain within the circle in Fig. 8 (b) includes some contributions of the conjugate spectrum term, and excludes high frequency information of the object field.

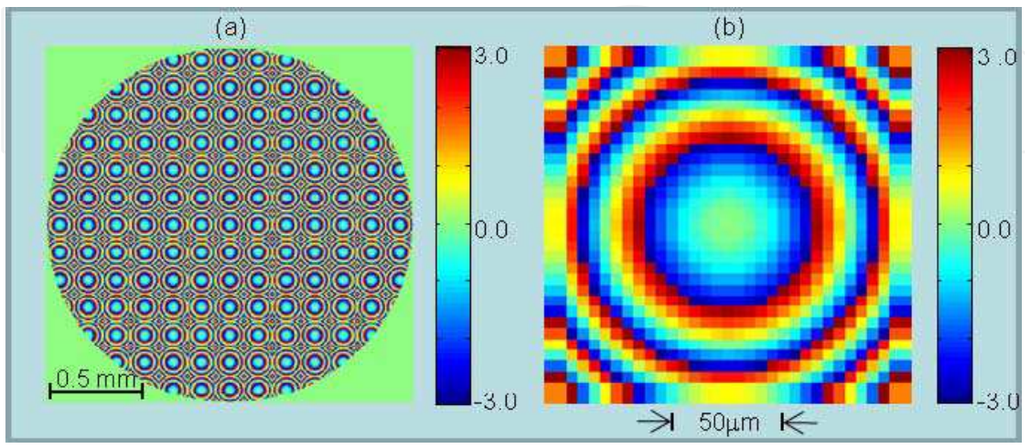

Fig. 7. (a) Wrapped phase modulation of the second test object formed by an array of micro lenses with focal length f=3mm. (b) Phase of a single lens in the array.

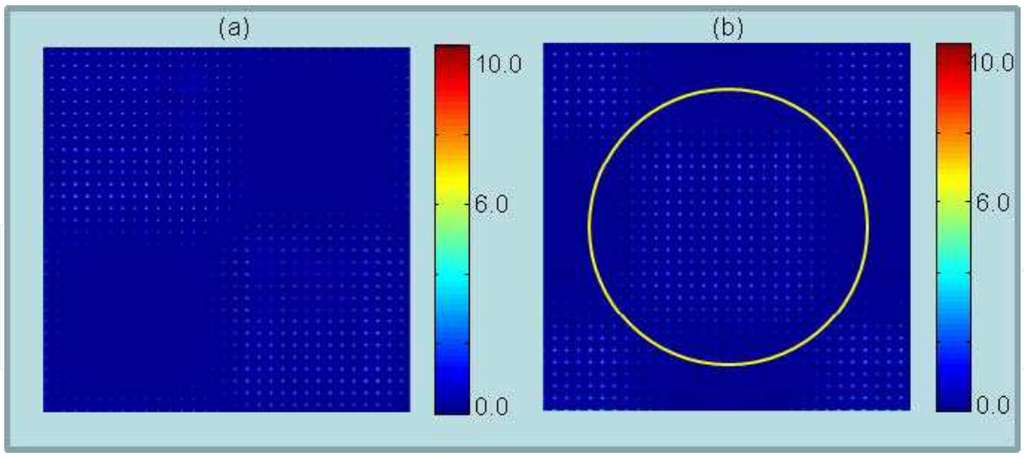

Fig. 8. Modulus of the hologram Fourier spectrum $H_m(u,v)$: (a) for the first modified hologram [Eq. (8)], and (b) for the second modified hologram [Eq. (13)].

To complete the FDSF process, we first obtain a filtered version, $h_f(x,y)$, of the second modified hologram $h_m(x,y)$, implementing the inverse Fourier transform of the spatially filtered hologram Fourier spectrum. The hologram $h_f(x,y)$ is formed essentially by the object term g(x,y), distorted with the part of the conjugate term which is not eliminated. We propagate the field $h_f(x,y)$ to the object plane, recovering an approximation of the object field. The wrapped phase of the recovered object field is shown in Fig. 9 (a), and a close view of the phase modulation of a single lens is displayed in Fig. 9 (b). In order to visualize more clearly the phase errors of this reconstruction, we display in Fig. 10 the central pixels of (a) the original object and (b) the reconstructed object, representing a reduced phase domain in the colour bar.

A quantitative evaluation of the reconstructed object field $f_R(x,y)$ can be made using the root mean square (RMS) error relation

$$\mathrm{Errf} = \sqrt{N_P^{-1} \sum_{\Omega_P} \frac{\left|f - f_R\right|^2}{\left|f\right|^2}}\,, \tag{14}$$

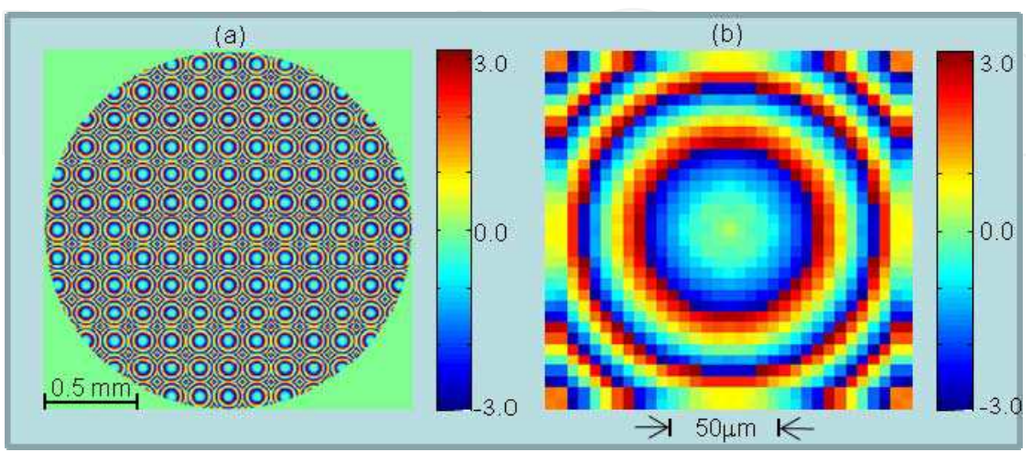

Fig. 9. (a) Wrapped phase modulation in the reconstructed object field, and (b) phase modulation at the central lens of the reconstructed object.

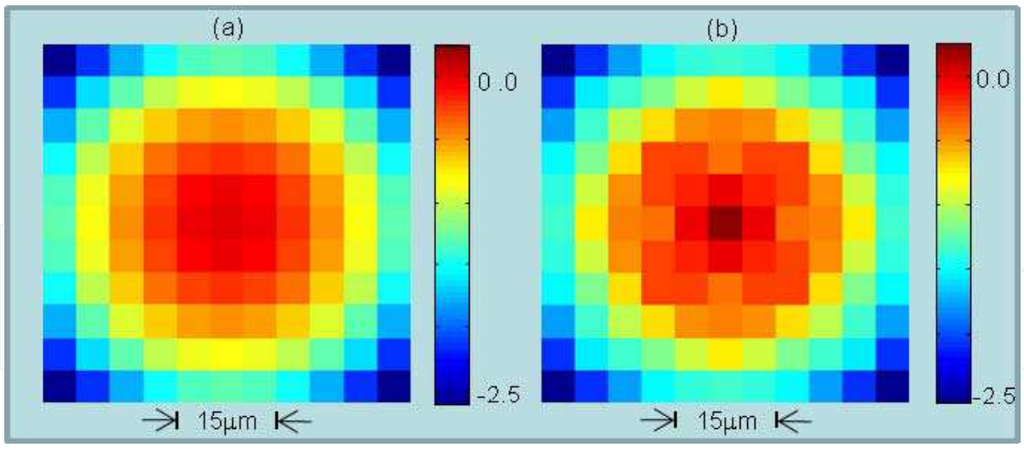

Fig. 10. Phase modulation at the central pixels of the original object (a), and at the corresponding pixels of the reconstructed object (b).

where f(x,y) is the true object field, N_P is the number of pixels in the object pupil Ω_P, and the summation is over the pixels in Ω_P. Eq. (14) provides a simultaneous evaluation of the error for both the modulus and the phase of the recovered field f_R. Although this error is dimensionless, Eq. (14) approximates a phase modulation error (in radians) if the modulus error $|f_R| - |f|$ is negligible. The error in the reconstruction of the second test object, computed with Eq. (14), is approximately 0.124.

Unfortunately, the error in Eq. (14) cannot be computed in an experimental reconstruction, for which the object complex field modulation f(x,y) is unknown. A convenient alternative to evaluate the reconstruction is to measure the RMS error of the field amplitude $|g_R|$ obtained at the CCD plane. This error is expressed as

$$\mathrm{Errg} = \sqrt{N_g^{-1} \sum_{\Omega g} \frac{\left[|g| - |g_R|\right]^2}{|g|^2}} \quad . \tag{15}$$

where $|g| = (I_g)^{1/2}$, I_g is the measured intensity in the LOADH setup when the RW is blocked out, Ω_g is the set of pixels in the CCD for which $|g| \neq 0$, and N_g is the number of pixels in the set Ω_g. Since the involved functions in Eq. (15) can be measured by the CCD, the error Errg is useful as an indirect measure of the reconstruction quality in a experimental situation.

2.2.1 Iterative error reduction algorithm in object reconstruction

The error in the reconstructed object field, obtained with the FDSF procedure applied in section 2.2, is partially due to the contributions of the conjugate term, contained within the area of the applied spatial filter [see Fig. 8 (b)]. Another source of error is the loss of high spatial frequencies of the object field due to the low-pass filtering. Next we describe a simple iterative algorithm that substantially reduces the reconstruction error.

A key procedure of the algorithm, which is referred to as iterative error reduction algorithm (ITERA), is the application of amplitude constraints in both the object and CCD planes. In the object plane the constraint is given by the support or pupil function p(x,y). Assuming that the transmittance of the object under study has constant modulus (=1), the amplitude of

the reconstructed field f_q (at the stage q of the process) is replaced by $(1+M_1|f_q|)/(M_1+1)$, which represents a weighted average of 1 and $|f_q|$, determined by a positive parameter M_1.
In the CCD plane the amplitude constraint is the modulus of the field propagated from the object alone, i. e. $|g|=(I_g)^{1/2}$, where I_g is the measured intensity in the LOADH setup when the RW is blocked out. At the q-th stage of the iterative process, the amplitude of the field g_q propagated to the CCD plane is replaced by $(|g|+M_2|g_q|)/(M_2+1)$, which is a weighted average of $|g|$ and $|g_q|$, determined by the positive parameter M_2.
The algorithm steps are schematically represented in Fig. 11. The input f_0 is the approximated reconstructed field, obtained with the FDSF procedure described in section 2.2. The positive numbers M_1 and M_2 determine the speed of adjustment of the field amplitude to the constraint amplitude. For example, for $M_1=0$ amplitude a_{q-1} at the object plane is replaced by the constraint amplitude, i.e. $a_q=1$. On the other hand for M=1, the amplitude a_{q-1} is replaced by $a_q=(1+a_{q-1})/2$. It is noted that large values of M_1 and M_2 tend to reduce the convergence speed, but they can be necessary to avoid fast stagnation. In the implemented ITERA we employ $M_1=20\alpha$ and $M_2=5\alpha$, where α takes the initial value of 1. During iterations, the value of α is made proportional to the evaluated error Errg (right block in Fig. 11).
In the block at the right side of Fig. 11, the operator PR represents the propagation to the CCD plane, and in the lower block, the operator PR^{-1} represents the back-propagation to the object plane.

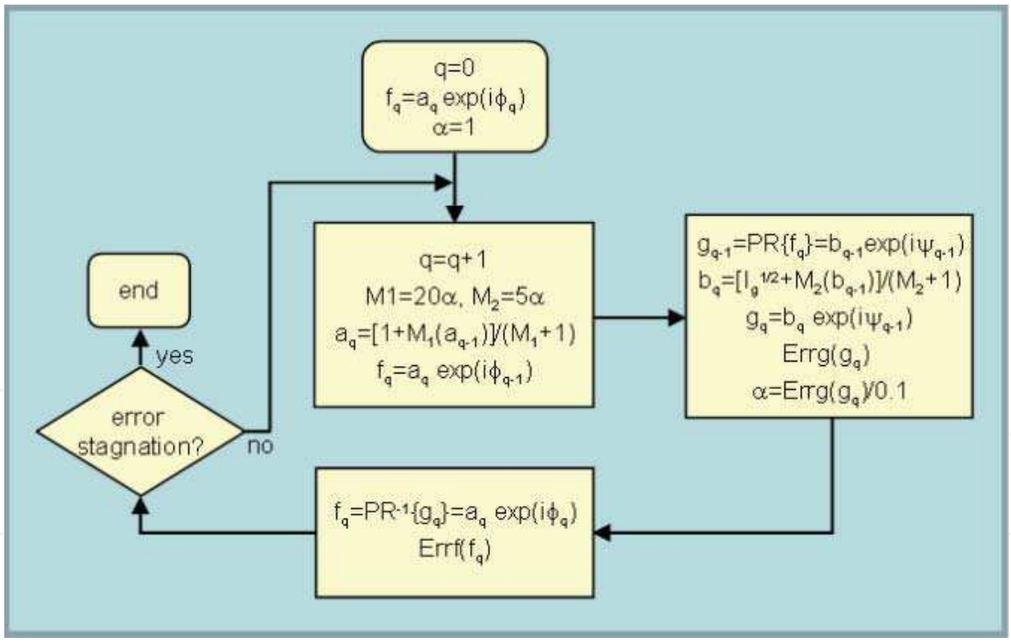

Fig. 11. Iterative error reduction algorithm (ITERA) for reducing the error in the first object field reconstruction.

We executed this algorithm using as input the reconstructed field obtained in section 2.2. The decrease of both errors Errf and Errg [Eqs. (14) and (15)], as a function of the iteration number, is shown in Fig. 12. The minimum errors obtained after 50 iterations are $Errf_{min}=0.001$ and $Errf_{min}=3.7x10^{-4}$, which represent a reduction of at least two magnitude orders in relation to the initial errors. The phase modulation at the central pixels of the

reconstructed field at the object plane, obtained for the numbers of iterations 8 and 50, are displayed in Fig. 13. The error Errf for these reconstructions corresponds to (a) the intermediate value 0.6 and (b) the minimum value 0.001. The quality of the final reconstruction can be visualized comparing Fig. 13 (b) with Fig. 10 (a).

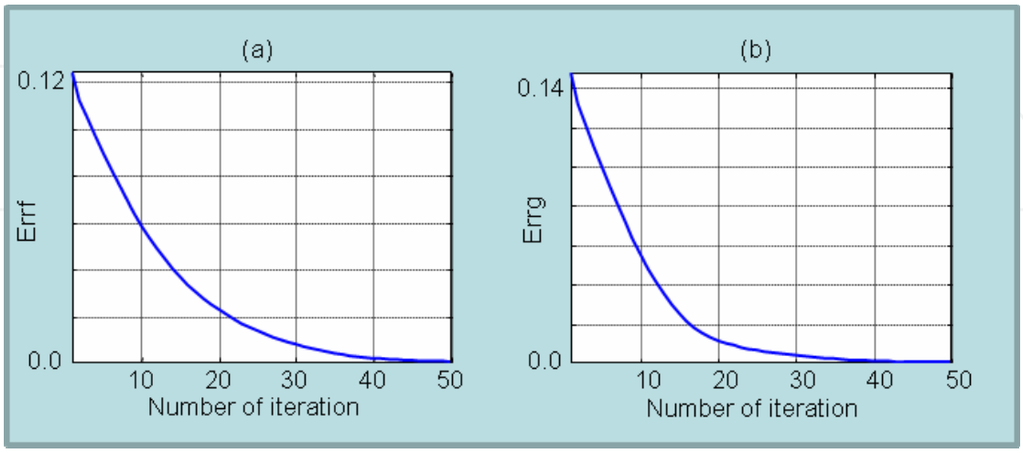

Fig. 12. Decrease of reconstruction errors (a) Errf and (b) Errg, as a function of the iteration number. The input is the first reconstructed object in section 2.2.

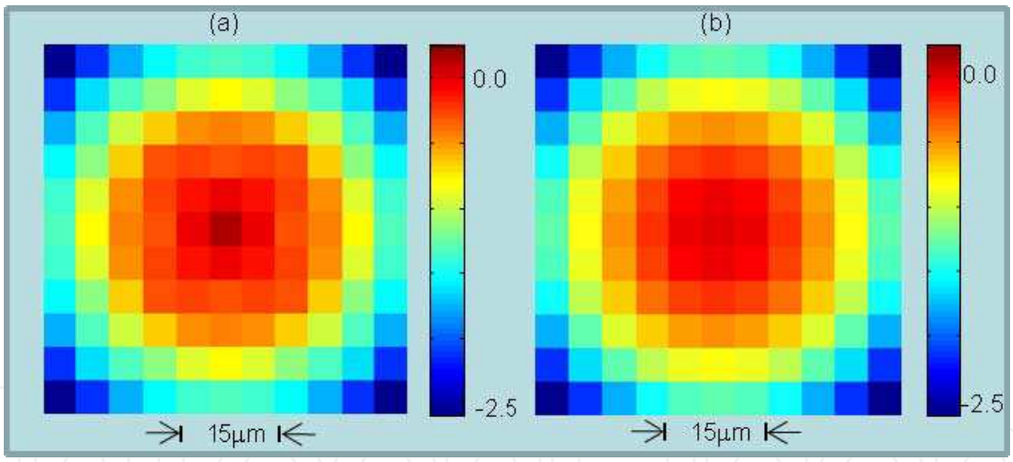

Fig. 13. Phase modulation at the central pixels of the reconstructed object field, obtained for the numbers of iterations (a) 8 and (b) 50.

2.2.2 Error reduction in an extremely noisy object reconstruction

To enhance the power of the ITERA algorithm, we consider a third test object whose BW is larger than the limit imposed by Eq. (11). This object is an array of micro lenses of focal distance f=1.5 mm, and a width W_L=125 μm. The pupil of the array of lenses has radius R=1 mm. The object bandwidth, obtained with the relation $BW_{OBJ}=(2)^{1/2}\ w_L\ (\lambda f)^{-1}$ is approximately 0.24, which exceeds the CCD BW in 20%. We employ the same setup and CCD parameters previously considered, except a new propagation distance z=31.25 mm. Fig. 14 shows the wrapped phase modulation (a) within the object pupil and (b) for the central lens of the array. We employ again a RW with spatial frequencies $u_0=v_0=BW_{CCD}/4$.

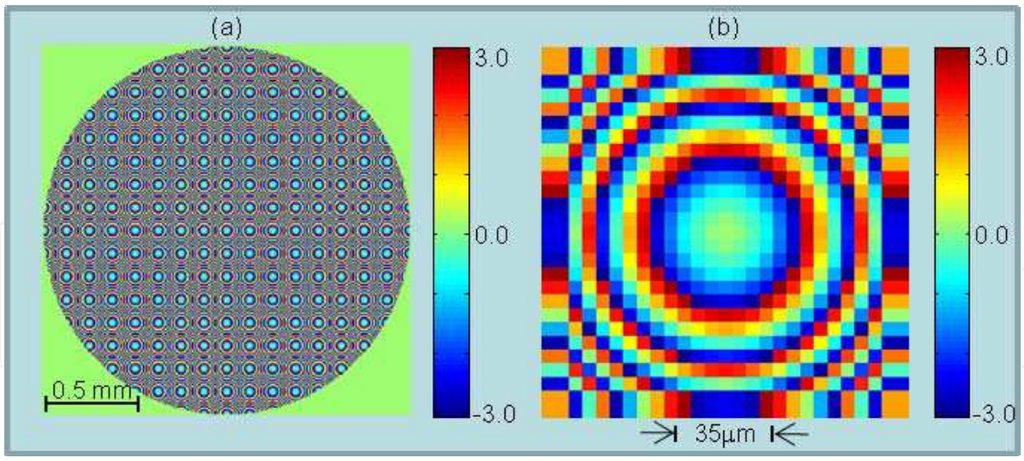

Fig. 14. (a) Wrapped phase modulation of the third test object formed by an array of micro lenses of focal length fL=1.5 mm. (b) Close view of the phase modulation in a single lens of the array.

After computing the propagated field, with Eq. (3), we obtained the second modified hologram $h_m(x,y)$ [Eq. (13)] and its Fourier spectrum $H_m(u,v)$. In the image of $|H_m(u,v)|$, displayed in Fig. (15), the object field term and the conjugate contribution appear highly overlapped. To make evident how these terms share the hologram spectrum space, we display the Fourier spectra for the separated terms $g(x,y)$ and $g^*(x,y)\exp[i4\pi(u_0x+v_0y)]$ that form $h_m(x,y)$. The modules of these Fourier spectra components are displayed in Fig. 16.
In spite of the severe overlapping of the object and conjugate terms in the Fourier spectrum of the hologram $h_m(x,y)$ [Fig. 15], we perform a first reconstruction using the FDSF method. The spatial filtering digitally eliminates the spectra information outside the circle shown in Fig. 15, whose diameter (in spatial frequency units) is DW_{CCD}=0.2 μm^{-1}. This spatial filtering is deficient by two reasons: it maintains a significant part of the conjugate contribution and it eliminates high frequency data of the object field. After performing the required steps of generating the spatially filtered hologram $h_m(x,y)$ and the propagation of this filtered

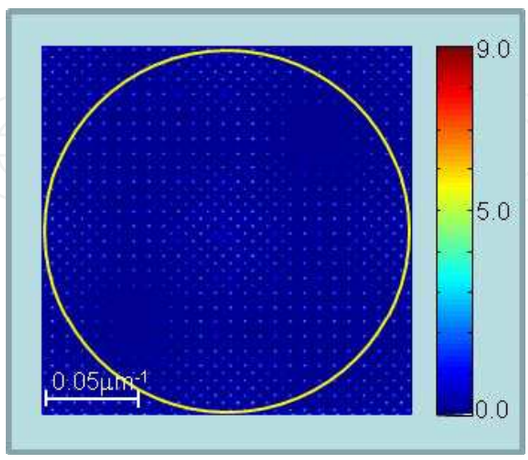

Fig. 15. Modulus of $H_m(u,v)$, for the second modified hologram [Eq. (13)], corresponding to the object field in Fig. 14. The spectrum contributions outside the yellow circle will be eliminated for the first reconstruction.

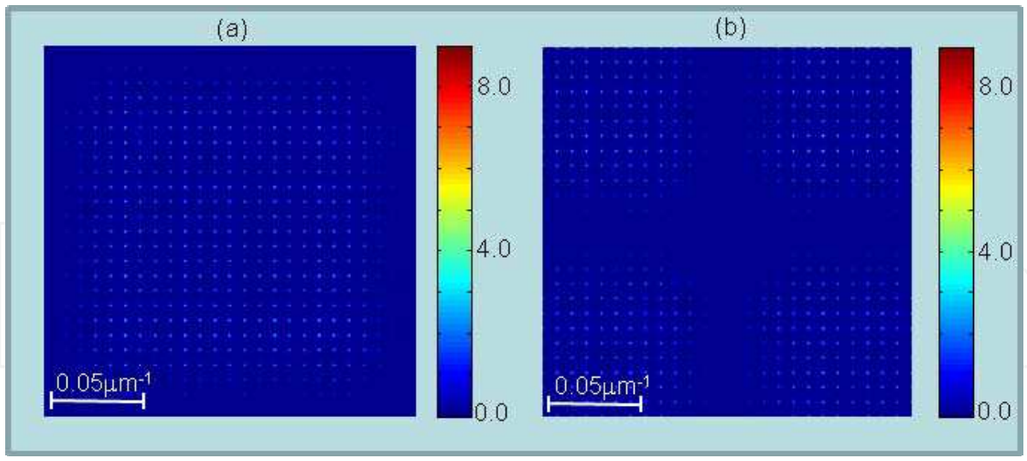

Fig. 16. Modules for the Fourier spectra of the separated terms (a) g(x,y) and (b) $g^*(x,y)\exp[i4\pi(u_0x+v_0y)]$, which form the modified hologram $h_m(x,y)$ of the test object.

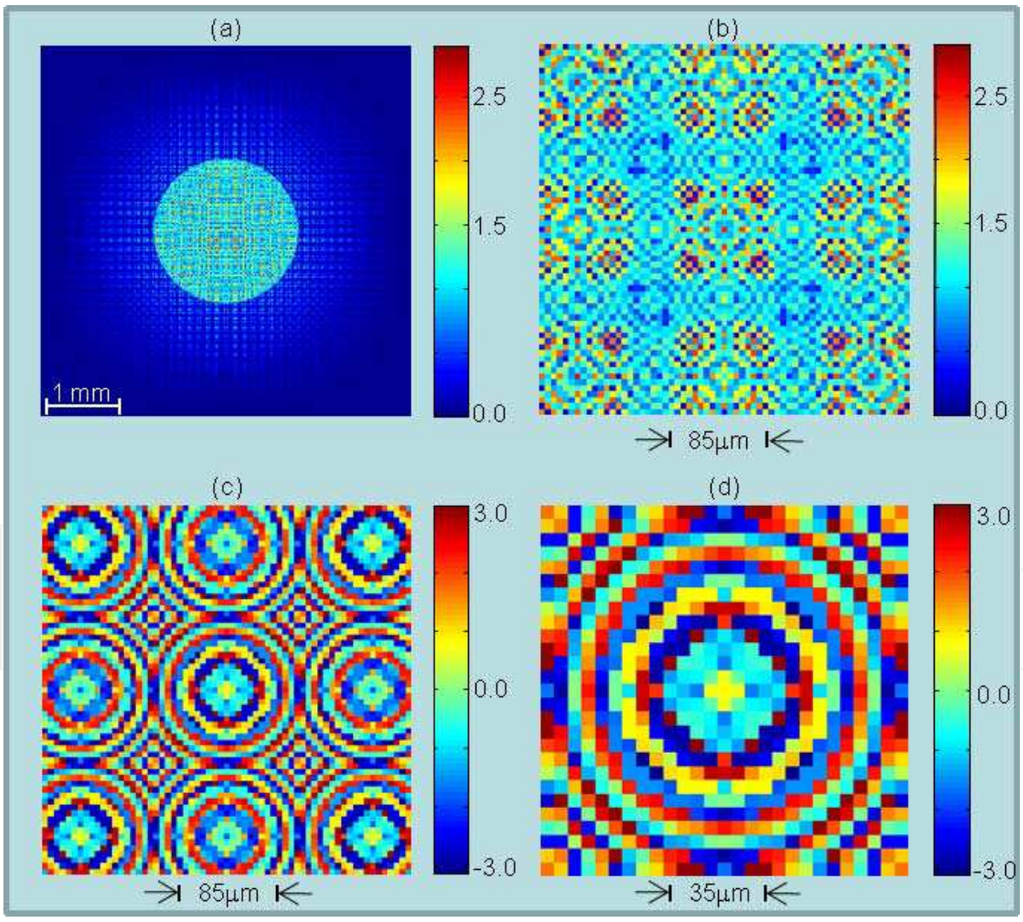

Fig. 17. First reconstruction of the third test object. Modulus of the field in (a) an extended and in (b) a close view. (c) Phase modulation of the central 9 micro lenses and (d) close view of the central lens phase modulation.

hologram to the object plane, we obtain the first reconstruction field. Fig. 17 (a,b) displays the amplitude of this reconstructed field, (c) the reconstructed phase modulation for the 9 central lenses of the array, and (d) a close view of the phase modulation in the central reconstructed lens. The object pupil, which is clearly seen in Fig. 17 (a), is polluted with a significant amount of light from the conjugate field, which fortunately appears out of focus. The detailed effect of the conjugate is observed in the close views of the amplitude (b) and phase modulation (c,d). Due to the presence of the conjugate field, the amplitude in Fig. 17 (a,b) takes values in the interval [0,2.9], which represents a large variation around the true object field amplitude A=1, within the pupil. On the other hand, the presence of the conjugate field also introduces a significant distortion in the phase of the reconstructed micro lenses (c,d). This distortion is evident when we compare the reconstructed lenses with the true lens phase modulation, shown in Fig. 14 (b).

We executed the ITERA algorithm with the same parameters employed in section 2.2.2, using as input the initial reconstructed field, described in the previous paragraph. The reduction of both errors Errf and Errg, as a function of the iteration number, is evidenced in Fig. 18. The minimum errors, obtained with 300 iterations, are $Errf_{min}$=0.01 and $Errf_{min}$= $6x10^{-4}$. Fig. 19 displays the reconstruction field amplitude and the phase modulation at the central reconstructed lens, at the end of the execution of ITERA. The negligible amplitude error within the reconstructed object pupil is consistent with the computed error $Errf_{min}$=0.01.

The low reconstruction error obtained in the present example makes evident that most of the noise introduced by the conjugated field is successfully eliminated by the application of ITERA. Now we wonder if the other error source, in the first reconstruction, namely the low-pass filtering of the object field, has been corrected or not. In other words we want to know if ITERA allows the recovery of the high frequency object features lost in the spatial filtering. Our answer to this significant question is yes. Fig. 20 (a) shows the object Fourier spectrum modulus $|F(u,v)|$, subject to the same low-pass filtering applied to the modified hologram (illustrated in Fig. 15). On the other hand, Fig. 20 (b) shows the modulus of the Fourier spectrum, $F_R(u,v)$, of the recovered field. It is remarkable that high frequency information which was eliminated in the object spectrum (Fig. 20 (a)) reappeared in the

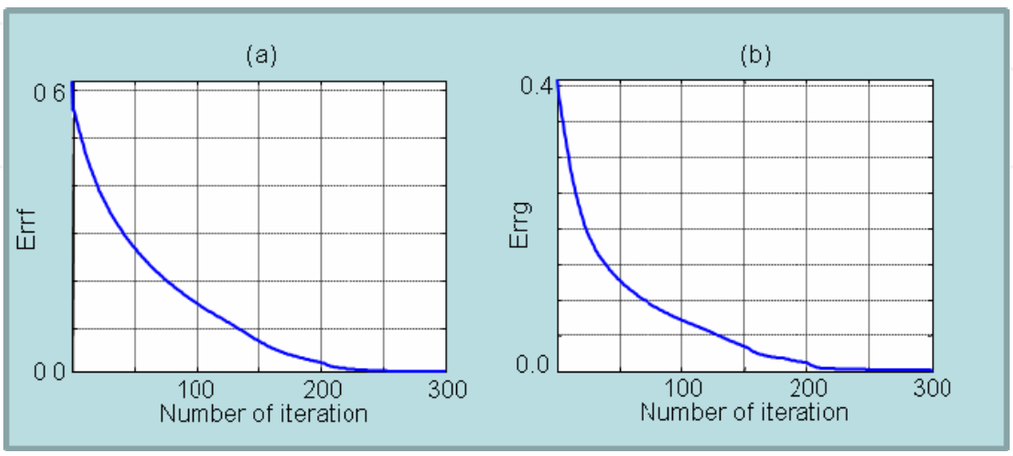

Fig. 18. Reduction of errors (a) Errf and (b) Errg, as a function of the iteration number, when the input is the first reconstructed object field, presented in Fig. 17.

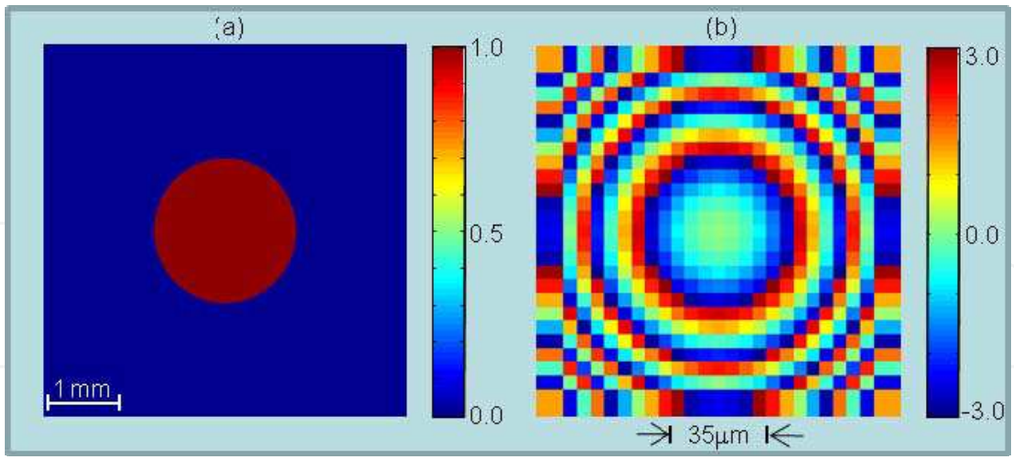

Fig. 19. (a) Modulus of the reconstructed object field, and (b) phase modulation at the central reconstructed micro lens, at the iteration 300 of the reducing error algorithm.

Fourier spectrum of the recovered object field (Fig. 20 (b)). This can be observed comparing the corners of both images in Fig. 20. We have verified the high fidelity of the recovered spatial frequency information $F_R(u,v)$ by a quantitative comparison with the Fourier spectrum F(u,v) of the test object.

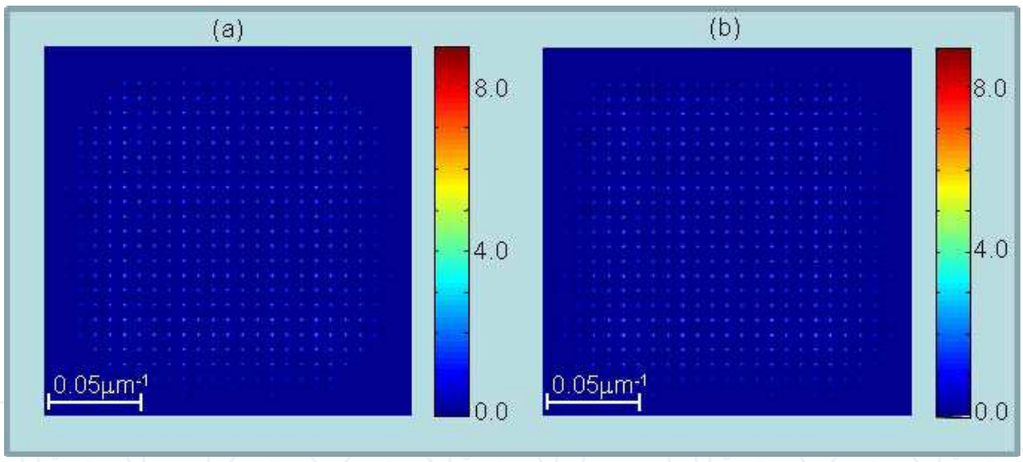

Fig. 20. Square root of the modules of (a) the spatially filtered object spectrum F(u,v), and (b) the Fourier spectrum $F_R(u,v)$, of the reconstructed object field $f_R(x,y)$.

3. Lensless on-axis digital holography without external reference wave

The error reduction algorithm (ITERA) described in section 2.2.1, has been successfully tested in the error reduction of large BW test objects, initially reconstructed by means of a FDSF technique. In the discussed cases it is assumed that the intensity information used for the reconstruction process is obtained in a LOADH optical setup. In this section we test the performance of ITERA applied to object field reconstruction in a RLOADH setup, schematically depicted in Fig. 21. In this setup, it is assumed that the object plane is illuminated by a plane wave and that the field scattered by the object freely propagates to the CCD plane.

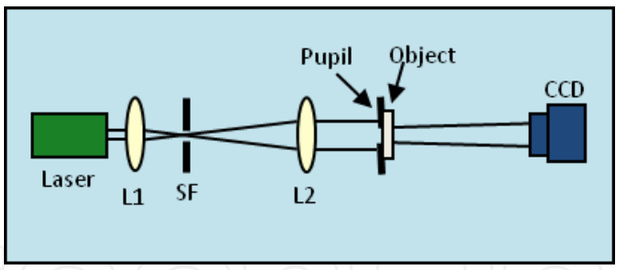

Fig. 21. RLOADH optical setup to implement DHM without an external reference wave.

We assume again that the object is limited by a pupil of binary transmittance p(x,y), and that the field transmitted at the object plane is given by Eq. (1). A common procedure used in DH, without an external RW, is to represent the object field by the expression

$$f(x,y) = p(x,y) + d(x,y) \tag{16}$$

where

$$d(x,y) = p(x,y)\{\exp[i\phi(x,y)] - 1\} . \tag{17}$$

The field propagated to the CCD plane, computed by means of the AS approach [Eq. (3)], can be expressed as

$$g(x,y) = g_p(x,y) + g_d(x,y) , \tag{18}$$

where $g_p(x,y)$ and $g_d(x,y)$ are the fields contributions from the object terms p(x,y) and d(x,y) respectively. Assuming a complete knowledge of the pupil function p(x,y), we can obtain, at least using numerical computation, the complex field $g_p(x,y)$. The intensity of the field g(x,y), or in-line hologram, can be measured by the CCD in the RLOADH setup. This intensity can be expressed as

$$h(x,y) = g_p g_p^* + g_d g_d^* + g_p g_d^* + g_p^* g_d . \tag{19}$$

Since we assume a complete knowledge of $g_p(x,y)$, we can obtain the modified hologram modulation

$$h_m(x,y) = \frac{h(x,y) - g_p g_p^*}{g_p^*} = g_d(x,y) + n(x,y) , \tag{20}$$

where

$$n(x,y) = \frac{g_d g_d^*}{g_p^*} + \frac{g_p g_d^*}{g_p^*} . \tag{21}$$

The division by $g_p^*(x,y)$ in Eqs. (20) and (21) is possible only in the region of the hologram where $g_p^*(x,y) \neq 0$. This is not an important restriction when the non-zero scattered field $g_d(x,y)$ occupies an area for which $g_p^*(x,y) \neq 0$. It is remarkable that the modified hologram

$h_m(x,y)$ is formed by the complex diffracted field $g_d(x,y)$ and the function n(x,y) that represents a noise term.

When the hologram modulation $h_m(x,y)$ is back-propagated to the object plane, the term $g_d(x,y)$ generates the function d(x,y), in a well defined region within the pupil. On the other hand, the structure of n(x,y) [Eq. (21)] makes unlikely that this term will produce well defined or focussed patterns within the pupil region. Thus we expect that the hologram back-propagation will allow the reconstruction of a good approximation to the field d(x,y). With this approximated version of d(x,y) we can obtain a first reconstruction of f(x,y) by means of Eq. (16). In the next section, we will discuss the reconstruction of a specific object, obtained from the modified in-line hologram given by Eq. (20). The error in this approximated reconstruction will be reduced by using the program ITERA, presented in section 2.2.1.

3.1 Reconstruction and error reduction in the RLOADH setup

To illustrate the reconstruction process using the modified in-line hologram presented in Eq. (20), we consider that the test object to be processed has the phase modulation of Fig. 22 (a). In this figure the large circle of radius R=1 mm corresponds to the object pupil p(x,y). The object field is zero outside this pupil. The phase modulation within the object pupil is zero except at the central circular region (whose radius is 200 μm.) that contains the phase modulation of a small array of micro lenses. A close view of this array of lenses is displayed in Fig. 22 (b). These micro lenses are identical to the ones employed in the example of section 2.2.2. The modulus of the field propagated to the CCD plane, when the object pupil is illuminated with a plane wave (of unitary amplitude), is displayed in Fig. 23 (a). In this case, the distance from the CCD to the object plane is z=20 mm. This distance was chosen to allow that most of the diffracted field $g_d(x,y)$ is covered by the field $g_p(x,y)$.

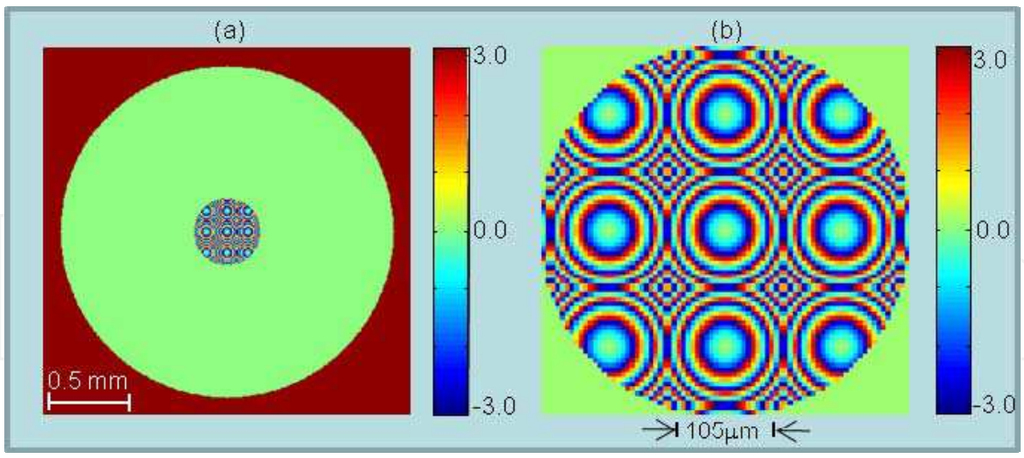

Fig. 22. (a) Phase modulation within the pupil of the fourth test object. (b) Close view of the small array of micro lenses at the center of the pupil.

For the generation of the modified in-line hologram [Eq. (20)] we only considered the region, $\Re_h$, where the amplitude of $g_p(x,y)$ is larger than 5% of its peak value. For the first reconstruction we omit the information outside this region. This is a practical method to avoid difficulties of division by g_p^* in Eq. (20). The modulus of the modified in-line hologram, displayed in Fig. 23 (b), shows the region $\Re_h$ (a circular domain) where this

hologram has been defined. A drawback of this method is that the information of g_d outside the region $\Re_h$, does not appear in the hologram. This missed information in function g_d corresponds to high spatial frequencies of the function d(x,y), in the object plane. An interesting feature of the reducing error algorithm ITERA, to be applied below, is that allow the recovery of the high frequency information of d(x,y), missed in the definition of the in-line hologram. Fig. 24 (a) shows the modules of functions g_p and g_d, respectively. It is noted (Fig. 24 (b)) that g_d contains information outside the region $\Re_h$ where the in-line hologram [Fig. 23 (b)] is defined.

After computing the modified in-line hologram $h_m(x,y)$ [Eq. (20)] we obtained the first reconstruction of function d(x,y). This is obtained by performing the back-propagation of the hologram to the object plane. The first reconstruction of the object field f(x,y), is obtained by adding the known function p(x,y) to the reconstructed function d(x,y). The amplitude and the phase of this reconstructed field, within the pupil domain, are shown in Fig. 25. The influence of noise is evident in the high amplitude variation shown in Fig. 25 (a). The

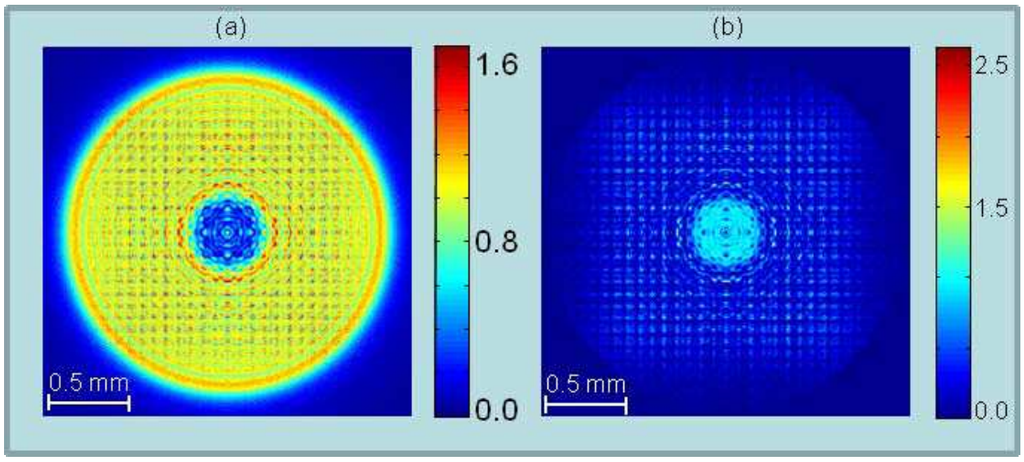

Fig. 23. (a) Amplitude of the object field, g(x,y), propagated to the CCD plane, and (b) modulus of the modified in-line hologram $h_m(x,y)$.

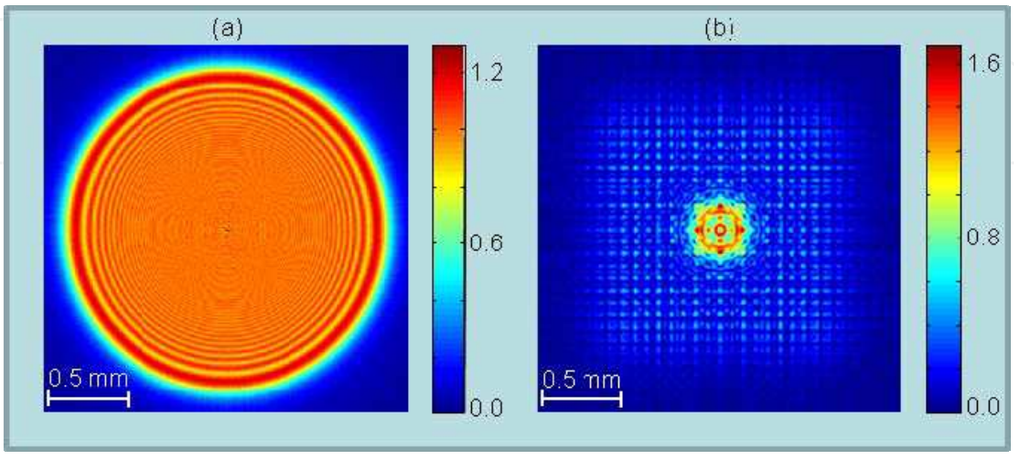

Fig. 24. Modules of the fields (a) $g_p(x,y)$ and (b) $g_d(x,y)$ that form the propagated object field g(x,y).

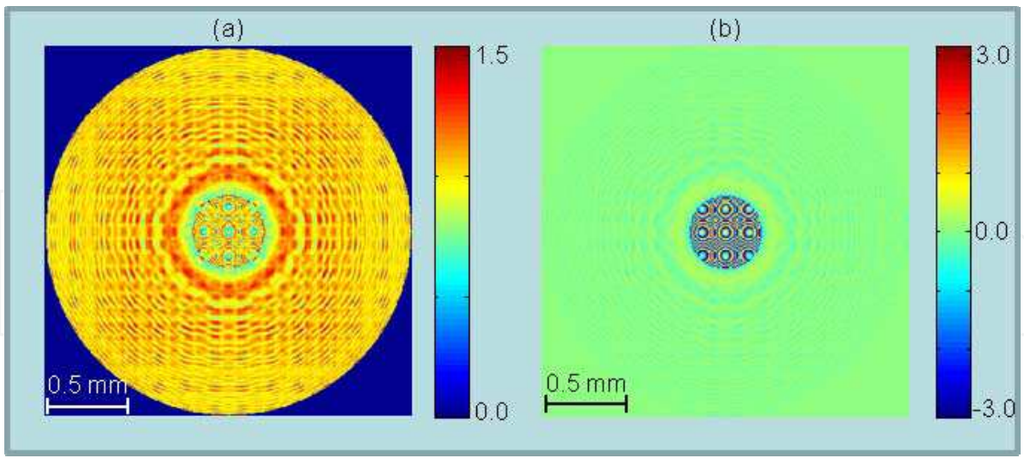

Fig. 25. Amplitude (a) and (b) phase of the first reconstruction of the object field (displayed in Fig. 22), obtained from the modified in-line hologram.

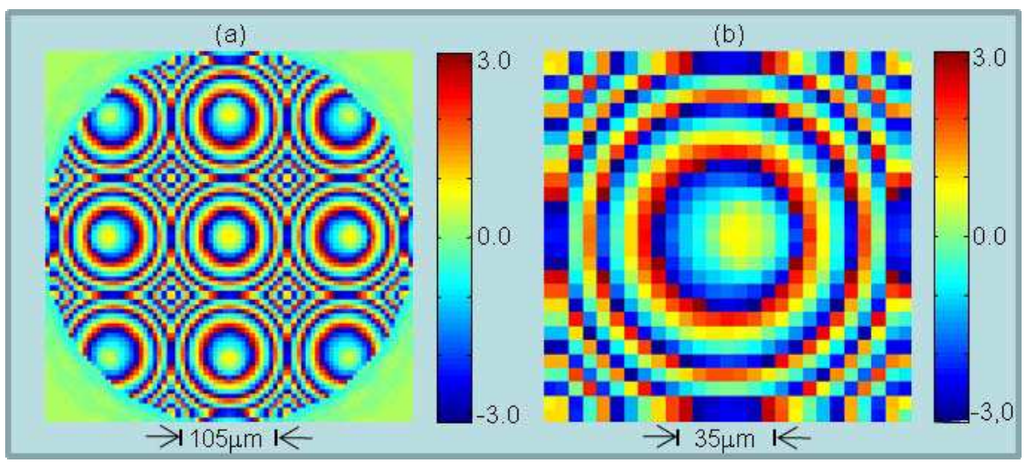

Fig. 26. (a) Phase modulation in the reconstructed array of lenses, and (b) close view of the phase modulation in the lens placed at the right side of the array, along the horizontal axis.

expected modulus within the pupil is A=1. A close view of the phase modulation in the array of lenses and is shown in Fig. 26 (a). The detailed image of a single lens, displayed in Fig. 26 (b), shows a clear asymmetry in the phase modulation.

We executed the ITERA program, with the parameters and constraints specified in section 2.2.1, using as input the first reconstructed object field mentioned in the previous paragraph. The reduction of errors Errf and Errg, as a function of the iteration number is displayed in Fig. 27. The error values (obtained at the iteration 185) are $Errf_{min}$=0.01 and $Errg_{min}$=0.0014 . We also computed the RMS error in the phase modulation obtaining 0.01 radians (at the iteration 185). As expected, this value coincides with the minimum value of Errf. The amplitude of the corrected object field, obtained at the iteration 185 of ITERA, is displayed in Fig. 28 (a). The corrected phase modulation of the asymmetrical lens in Fig. 27 (b) is displayed in Fig. 28 (b).

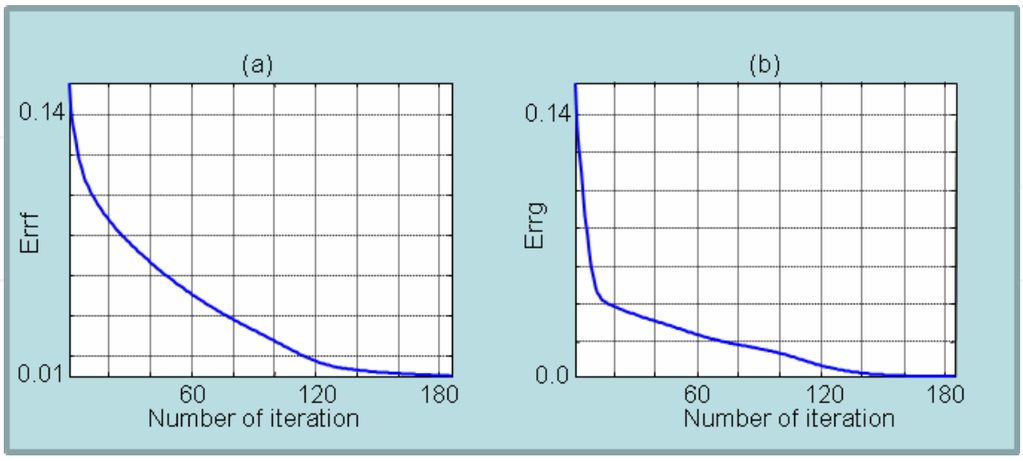

Fig. 27. (a) Reduction of errors (a) Errf and (b) Errg, as a function of the iteration number, when the input is the first reconstructed object field, presented in Fig. 25.

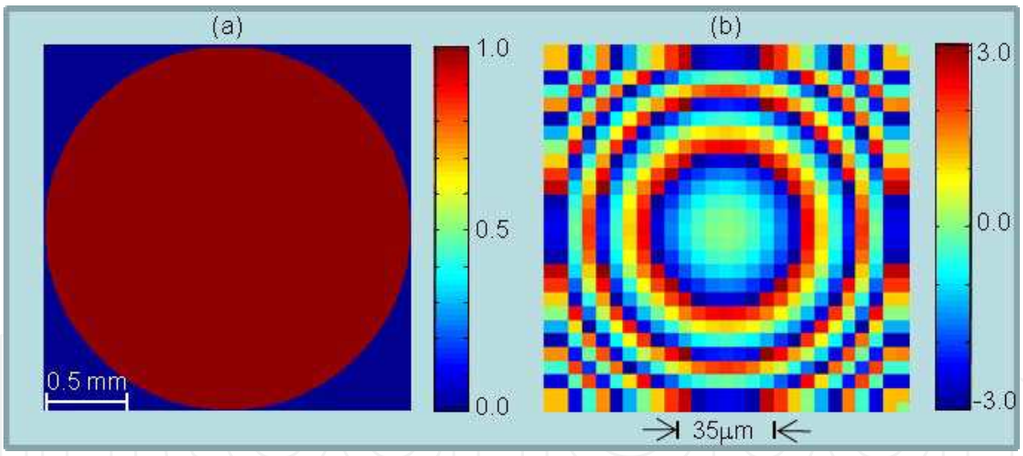

Fig. 28. (a) Amplitude of the reconstructed object field after the iteration 185, and (b) close view of the corrected version of the asymmetrical lens displayed in Fig. 26 (b).

The algorithm ITERA, applied to the object field reconstructions performed in the present and previous sections, have employed the adjusting parameters $M_1 = 20\alpha$ and $M_2 = 5\alpha$ (see Fig. 11). We note that the convergence speed of ITERA can be optimized by different definitions of these parameters. For example, in the application of ITERA to the reconstruction in this section, the error reduction obtained in Fig. 27, is also obtained with only 105 iterations, employing the parameters $M_1 = 6\alpha$ and $M_2 = 2\alpha$. The evolution of errors Errf and Errg, with these new parameters M_1 and M_2, is shown in Fig. 29.

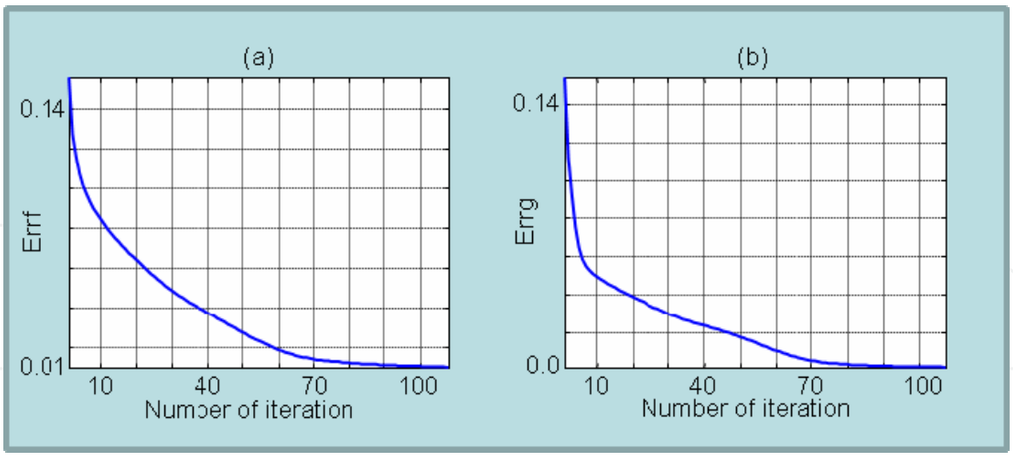

Fig. 29. (a) Reduction of errors (a) Errf and (b) Errg, as a function of the iteration number, using modified adjustment parameters M_1 and M_2.

4. Conclusion

We have implemented and tested an algorithm (ITERA) for reducing the error in the reconstruction of large BW object fields performed with intensity data from the LOADH and RLOADH optical setups. The initial step is the generation of a first reconstruction which is a good approximation of the true object field.

In the case of the LOADH setup, the first reconstruction is obtained by a FDSF method, based on the use of a modified hologram that contains the object field contribution on-axis, and the conjugate of this field off-axis. The contribution of the conjugate term in the hologram is reduced by spatial filtering in the hologram Fourier domain. On the other hand, when the modified filtered hologram is back-propagated to the object plane, the conjugated term appears defocused in this plane.

For the first reconstruction in the RLOADH setup we proposed a modified in-line hologram that essentially contains the object field information (in the CCD plane) and a noise term. An advantageous feature of the modified in-line hologram is that the term corresponding to the object field appears well focussed during propagation to the object plane, while the noise term appears defocused. This feature propitiates a dilution of the noise in the first reconstruction, within the object pupil.

The ITERA program allows a significant error reduction in both initial reconstructions. The good performance of ITERA is due in part to the relatively low noise of initial reconstructions. Another factor that also propitiates a fast convergence without stagnation is the gradual applications of constraints. Specifically, during a given iteration the obtained amplitude field a(x,y) (either at the object plane or the CCD plane) is replaced by a weighted average of the amplitude constraint with the field a(x,y).

A remarkable feature of ITERA is that it allows the recovery of high frequency information of the object field, which is lost in the first reconstruction. In the considered examples, it was possible to make negligible the reconstruction error at the end of application of ITERA, with a moderate number of iterations. The convergence speed of the algorithm can be optimized by the appropriate choice of the adjustment parameters M_1 and M_2.

5. References

Arrizón V. & Sánchez-de-la-Llave D., (2004). Common-path interferometry with one-dimensional periodic filters. *Opt. Lett.,* Vol. 29, No. 2, (Jan. 2004) 141-143, ISSN 0146-9592, 1539-4794.

Arrizón V., Testorf M., Sinzinger S., & Jahns J., (2000). Iterative optimization of phase-only diffractive optical elements based on a lenslet array. *J. Opt. Soc. Am. A,* Vol. 17, No. 12, (Dec. 2000) 2157-2164, ISSN 1084-7529, 1520-8532.

Car D.l, Kemper B., Wernicke G., & von Bally G. (2004). Parameter-Optimized Digital Holographic Microscope for High-Resolution Living-Cell Analysis. *Appl. Opt.,* Vol. 43, No. 36, (Dec. 2004) 6536-6544, ISSN 1559-128X , 2155-3165.

Cederquist J. N., Fienup J.R., Wackerman C. C., Robinson S. R., & Kryskowski D. (1989). Wave-front phase estimation from Fourier intensity measurements. *J. Opt. Soc. Am. A*, Vol. 6, No. 7, (Jul. 1989) 1020-1026, ISSN 1084-7529, 1520-8532.

Charrière F., Pavillon N., Colomb T., Depeursinge C., Heger T. J., Mitchell E. A. D., Marquet P., & Rappaz B. (2006). Living specimen tomography by digital holographic microscopy: morphometry of testate amoeba. *Opt. Express,* Vol. 14, No.16, (Aug. 2006) 7005-7013, ISSN 1094-4087.

Colomb T., Cuche E., Charrière F., Kühn J., Aspert N., Montfort F., Marquet P., & Depeursinge C. (2006). Automatic procedure for aberration compensation in digital holographic microscopy and applications to specimen shape compensation. *Appl. Opt.,* Vol. 45, No. 5, (Feb. 2006) 851-863, ISSN 1559-128X.

Cruz, M.L.; Castro, A. & Arrizón, V. (2008). Phase retrieval in digital holographic microscopy using a Gerchberg-Saxton algorithm, *Proceedings of Optics and Photonics for Information Processing II,* pp. 70721C, ISBN 0277-786X, USA, Sept. 2008, SPIE, San Diego, CA..

Cruz M.L., Castro A., & Arrizón A. (2009) Phase shifting digital holography implemented with a twisted-nematic liquid-crystal display. *Appl. Opt.,* Vol. 48, No. 36, (Dec. 2009) 6907-6912, ISSN 1559-128X.

Denis L., Fournier C., Fournel T., Ducottet C. (2005). Twin-image noise reduction by phase retrieval in in-line digital holography, *Proceedings of Wavelets XI* , Vol. 5914, 59140J, ISBN 9780819459190, USA, (Jul., 2005), SPIE , San Diego, CA..

Ferraro P., De Nicola S., Finizio A., Coppola G., Grilli S., Magro C., & Pierattini G. (2003). Compensation of the Inherent Wave Front Curvature in Digital Holographic Coherent Microscopy for Quantitative Phase-Contrast Imaging. *Appl. Opt.,* 42, Vol. 42, No. 11, (Apr. 2003) 1938-1946 , ISSN 1559-128X.

Ferraro P., Grilli S., Alfieri D., De Nicola S., Finizio A., Pierattini G., Javidi B., Coppola G., & Striano V. (2005). Extended focused image in microscopy by digital Holography. *Opt. Express* , Vol. 13, No. 18, (Sep., 2005) 6738-6749, ISSN 1094-4087.

Fienup J. R., (1987). Reconstruction of a complex-valued object from the modulus of its Fourier transform using a support constraint. *J. Opt. Soc. Am. A,* Vol. 4, No. 1, (Jan., 1987) 118-123, ISSN 1084-7529.

Garcia-Sucerquia J., Xu W., Jericho K. Klages P., Jericho M. H., & Kreuzer J. (2006). Digital in-line holographic microscopy. *Appl. Opt.*, Vol. 45, No. 5, (Feb. 2006) 836-850, ISSN 1559-128X.

Goodman J. W., (1996), *Introduction to Fourier Optics*, Roberts McGraw Hill Higher Education, 2nd edition, ISBN-10 0071142576, USA.

Guo H., Yu Y. & Chen M. (2007). Blind phase shift estimation in phase-shifting interferometry. *J. Opt. Soc. Am. A,* Vol. 24, No. 1, (Jan. 2007) 25-33, ISSN 1084-7529.

Haddad, W. S., Cullen, D., Solem, J. C, Longworth, J. W., McPherson, A., Boyer, K., & Rhodes, C. K. (1992). Fourier-Transform Holographic Microscope. *Appl. Opt.*, Vol. 31, No. 24, (Aug. 1992) 4973-4978, ISSN 1559-128X.

Hwang H., & Han P. (2007). Signal reconstruction algorithm based on a single intensity in the Fresnel domain. *Opt. Express,* Vol. 15, No. 7, (Apr. 2007) 3766-3776, ISSN 1094-4087.

Javidi B., Inkyu M, Yeom S., & Carapezza E. (2005). Three-dimensional imaging and recognition of microorganism using single-exposure on-line (SEOL) digital holography. *Opt. Express,* Vol. 13, No. 12. (Jun. , 2005) 4492-4506, ISSN 1094-4087.

Javidi B., Yeom S., Moon I., & Daneshpanah M. (2006). Real-time automated 3D sensing, detection, and recognition of dynamic biological micro-organic events. *Opt. Express,* Vol. 14, No. 9, (May 2006) 3806-3829, ISSN 1094-4087.

Kreis T. (1986). Digital holographic interference-phase measurement using the Fourier-transform method. *J. Opt. Soc. Am. A*, Vol. 3, No. 6, (Jun. 1986) 847-855, ISSN 1084-7529.

Liebling M., Blu T., & Unser M. (2004). Complex-wave retrieval from a single off-axis hologram. *J. Opt. Soc. Am. A,* Vol. 21, No. 3, (Mar. 2004) 367-377 , ISSN 1084-7529.

Mann C., Yu L., Lo C., & Kim M. (2005). High-resolution quantitative phase-contrast microscopy by digital holography. *Opt. Express,* Vol. 13, No. 22, (Oct. 2005) 8693-8698, ISSN 1094-4087.

Marquet P., Rappaz B., Magistretti P. J., Cuche E., Emery Y., Colomb T., & Depeursinge C. (2005). Digital holographic microscopy: a noninvasive contrast imaging technique allowing quantitative visualization of living cells with subwavelength axial accuracy. *Opt. Lett.,* Vol. 30, No. 5, (Mar, 2005) 468-470, ISSN 0146-9592.

Meneses-Fabian C., Rodriguez-Zurita G., & Arrizón V. (2006). Optical tomography of transparent objects with phase-shifting interferometry and stepwise-shifted Ronchi ruling. *J. Opt. Soc. Am. A,* Vol. 23, No. 2, (Feb. 2006) 298-305, ISSN 1084-7529, 1520-8532.

Morlens A.S., Gautier J., Rey G. , Zeitoun P. , Caumes J.P., Kos-Rosset M. , Merdji H. , Kazamias S. , Cassou K., & Fajardo M. (2006). Submicrometer digital in-line holographic microscopy at 32 nm with high-order harmonics. *Opt. Express,* Vol. 31, NO. 21, (Nov. 2006) 3095-3097, ISSN 1094-4087.

Nakamura T., Nitta K., & Matoba O. (2007). Iterative algorithm of phase determination in digital holography for real-time recording of real objects. *Appl. Opt.*, Vol. 46, No. 28, (Oct. 2007) 6849-6853, ISSN 1559-128X , 2155-3165.

Oh C., Isikman S. O., Khademhosseinieh B., & Ozcan A. (2010). On-chip differential interference contrast microscopy using lensless digital holography. *Opt. Express,* Vol. 18, No. 5, (Mar. 2010) 4717-4726, ISSN 1094-4087.

Pedrini G., Fröning P., Fessler H., & Tiziani H.J. (1998). In-Line Digital Holographic Interferometry. *Appl. Opt.,* Vol. 37, No. 26, (Sept. 1998) 6262-6269, ISSN 1559-128X, 2155-3165.

Pedrini G., Fröning P., Tiziani H.J., & Mendoza Santoyo F. (1999). Shape measurement of microscopic structures using digital holograms. *Optics Commun.*, Vol. 164, No. 4-6, (Jun. 1999) 257-268, ISSN 0030-4018.

Qian K., Fu Y., Liu Q., Seah H. S., & Asundi A. (2006). Generalized three-dimensional windowed Fourier transform for fringe analysis. *Opt. Lett.*, Vol. 31, No. 14, (Jul. 2006) 2121-2123, ISSN 0146-9592, 1539-4794.

Rappaz B., Marquet P., Cuche E., Emery Y., Depeursinge C., & Magistretti P. (2005). Measurement of the integral refractive index and dynamic cell morphometry of living cells with digital holographic microscopy. *Opt. Express*, Vol. 13, No. 23, (Nov. 2005) 9361-9373, ISSN 1094-4087.

Repetto L. , Piano E., & Pontiggia C., (2004). Lensless digital holographic microscope with light-emitting diode illumination. *Opt. Lett.*, Vol. 29, No. 10, (May. 2004) 1132-1134, ISSN 0146-9592, 1539-4794.

Schnars U., & Jüptner W. (2002). Digital recording and numerical reconstruction of holograms. *Meas. Sci. Technol.,* Vol. 13, No. 9, (Sept. 2002), R85, ISSN 0957-0233, 1361-6501.

Singh V. R. & Asundi A. (2009). In-line digital holography for dynamic metrology of MEMS. *Chin. Opt. Lett.,* Vol. 7, No. 12, (Dec. 2009) 1117-1122.

Takeda M., Ina H., & Kobayashi S. (1982). Fourier-transform method of fringe-pattern analysis for computer-based topography and interferometry. *J. Opt. Soc. Am.,* Vol. 72, No. 1, (Jan. 1982) 156-160, ISSN 1084-7529, 1520-8532.

Wagner C., Seebacher S., Osten W., & Jüptner W. (1999). Digital Recording and Numerical Reconstruction of Lensless Fourier Holograms in Optical Metrology. *Appl. Op*t. 38, No. 22, (Aug. 1999) 4812-4820, ISSN, 1559-128X , 2155-3165.

Wu J. S., Weierstall U., Spence J. C. H., & Koch C. T. (2004). Iterative phase retrieval without support. *Opt. Lett.,* Vol. 29, No. 23, (Dec., 2004) 2737-2739, ISSN 0146-9592, 1539-4794.

Xu W., Jericho M. H., Meinertzhagen I. A., & Kreuzer H. J. Digital In-Line Holography of Microspheres. *Appl. Opt.,* Vol. 41, No. 25, (Sept. 2002) 5367-5375, ISSN 1559-128X , 2155-3165.

Yamaguchi I. & Zhang T. (1997). Phase-shifting digital holography. *Opt. Lett.,* Vol. 22, No. 16, (Aug. 1997) 1268-1270, ISSN 0146-9592, 1539-4794.

Yamaguchi I., Kato J., Ohta S., & Mizuno J. (2001). Image formation in phase-shifting digital holography and applications to microscopy. *Appl. Opt.*, Vol. 40, No. 34, (Dec. 2001) 6177-6186, ISSN 1559-128X , 2155-3165.

Zhang T. & Yamaguchi I. (1998). Three-dimensional microscopy with phase-shifting digital holography. *Opt. Lett.*, Vol. 23, No. 15, (Aug, 1998) 1221-1223, ISSN 0146-9592, 1539-4794.

Holography, Research and Technologies

Edited by Prof. Joseph Rosen

ISBN 978-953-307-227-2
Hard cover, 454 pages
Publisher InTech
Published online 28, February, 2011
Published in print edition February, 2011

Holography has recently become a field of much interest because of the many new applications implemented by various holographic techniques. This book is a collection of 22 excellent chapters written by various experts, and it covers various aspects of holography. The chapters of the book are organized in six sections, starting with theory, continuing with materials, techniques, applications as well as digital algorithms, and finally ending with non-optical holograms. The book contains recent outputs from researches belonging to different research groups worldwide, providing a rich diversity of approaches to the topic of holography.

How to reference

In order to correctly reference this scholarly work, feel free to copy and paste the following:

Victor Arrizón, Ulises Ruiz and Maria Luisa Cruz (2011). Iterative Noise Reduction in Digital Holographic Microscopy, Holography, Research and Technologies, Prof. Joseph Rosen (Ed.), ISBN: 978-953-307-227-2, InTech, Available from: http://www.intechopen.com/books/holography-research-and-technologies/iterative-noise-reduction-in-digital-holographic-microscopy

INTECH
open science | open minds

InTech Europe
University Campus STeP Ri
Slavka Krautzeka 83/A
51000 Rijeka, Croatia
Phone: +385 (51) 770 447
Fax: +385 (51) 686 166
www.intechopen.com

InTech China
Unit 405, Office Block, Hotel Equatorial Shanghai
No.65, Yan An Road (West), Shanghai, 200040, China
中国上海市延安西路65号上海国际贵都大饭店办公楼405单元
Phone: +86-21-62489820
Fax: +86-21-62489821

IntechOpen